Structural Biology and Molecular Biophysics
Plant Biology

Reviewed Preprint
v1 • November 18, 2024
Not revised

Molecular dynamics simulations illuminate the role of sequence context in the ELF3-PrD-based temperature sensing mechanism in plants

Richard J Lindsay, Rafael Giordano Viegas, Vitor BP Leite, Philip A Wigge, Sonya M Hanson

Center for Computational Biology, Flatiron Institute, New York, USA • Center for Computational Mathematics, Flatiron Institute, New York, USA • Department of Physics, São Paulo State University (UNESP), Institute of Biosciences, Humanities and Exact Sciences, São Paulo, Brazil • Federal Institute of Education, Science and Technology of São Paulo (IFSP), São Paulo, Brazil • Leibniz-Institut für Gemüse-und Zierpflanzenbau, Großbeeren, Germany • Institute of Biochemistry and Biology, University of Potsdam, Potsdam, Germany

eLife Assessment

In this potentially **valuable** computational study, the authors conducted atomistic and coarse-grained simulations to probe the temperature-dependent phase behaviors of ELF3, a disordered component of the evening complex in plant. The results aim to highlight the role of polyQ tracts in modulating the temperature sensitivity. The level of evidence is considered **incomplete**, due to the lack of systematic calibration of the coarse-grained model and limited statistical uncertainty analysis, especially considering the relatively subtle nature of the differences due to temperature change.

https://doi.org/10.7554/eLife.102410.1.sa3

Abstract

The evening complex (EC) is a tripartite DNA repressor and a core component of the circadian clock that provides a mechanism for temperature-responsive growth and development of many plants. ELF3, a component of the EC, is a disordered scaffolding protein that blocks transcription of growth genes at low temperature. At increased temperature EC DNA binding is disrupted and ELF3 is sequestered in a reversible nuclear condensate, allowing transcription and growth to proceed. The condensation is driven by a low complexity prion-like domain (PrD), and the sensitivity of the temperature response is modulated by the length of a variable polyQ tract, with a longer polyQ tract corresponding to enhanced condensate formation and hypocotyl growth at increased temperature. Here, a series of computational studies provides evidence that polyQ tracts promote formation of temperature-sensitive helices in flanking residues with potential impacts for EC stability

under increasing temperature. REST2 simulations uncover a heat-induced population of condensation-prone conformations that results from the exposure of 'sticky' aromatic residues by temperature-responsive breaking of long-range contacts. Coarse-grained Martini simulations reveal both polyQ tract length and sequence context modulate the temperature dependence of cluster formation. Understanding the molecular mechanism underlying the ELF3-PrD temperature response in plants has implications for technologies including modular temperature-response elements for heat-responsive protein design and agricultural advances to enable optimization of crop yields and allow plants to thrive in increasingly inhospitable environments.

Introduction

Temperature sensing mechanisms are critical to the survival of all life, but for plants, which are mostly stationary and yet flourish in a vast array of climates and seasonal variations, temperature sensors have a key, yet still poorly understood, role. While plants have diverse schemes to survive and thrive at a broad range of temperatures, such as vernalization, heat stress, and cold stress (Kerbler and Wigge, 2023), one mechanism that is more specific to plants is thermomorphogenesis, or when plants adjust their morphology in response to temperature (Quint et al., 2016).

Several thermosensory biomolecules have been identified, like the temperature-responsive uncoiling of chromatin, bending of DNA to increase gene transcription, and the melting of hairpin loops in RNA to enhance protein expression (Paik and Huq, 2019; Lin et al., 2020; Sengupta and Garrity, 2013). One specific component known to be involved in thermomorphogenesis is the Evening Complex (EC), whose function depends on protein-protein and protein-DNA interactions, and has been well-studied in *Arabidopsis thaliana*. The EC is conserved in land plants (Liu et al., 2001) and is a tripartite protein complex that provides a tunable temperature-sensing mechanism with implications for growth rate, flowering, and potentially senescence and circadian rhythm (Zagotta et al., 1992; Anwer et al., 2014; Nusinow et al., 2011; Thines and Harmon, 2010; Box et al., 2015; Jung et al., 2020). Understanding the molecular basis for the temperature sensing mechanism of the Evening Complex has implications on a warming planet where even a 1ºC rise in temperature would affect crop yield (Zhao et al., 2017).

The EC is a transcription repressor with three known protein components – ELF3, ELF4, and LUX ARRYTHMO – where LUX is a transcription factor (Nusinow et al., 2011; Zhang et al., 2019), ELF4 is a small helical protein responsible for stabilizing the complex, and ELF3 is a large mostly disordered protein that sequesters into reversible nuclear condensates at high temperatures (**Fig. 1A**) resulting in the release of the rest of the repressor complex, allowing the expression of growth genes (Jung et al., 2020). While ELF3 is a 695 residue long intrinsically disordered protein (IDP) the C-terminal prion-like domain (PrD), first recognized by Jung et al. (2020), is necessary and sufficient for condensate formation (**Fig. 1C**) and makes up a quarter of the ELF3 sequence (residues 492 to 664 out of 695 total residues) (Jung et al., 2020). Prion-like domains are identified by matching sequence patterns found initially in amyloid-forming prions, namely via an enrichment in polar amino acids like glutamine and asparagine (Lancaster et al., 2014), but this has proved a successful way of identifying low-complexity domains that are indicative of disordered protein regions (Romero et al., 2001). The PrD in ELF3 (hereafter referred to as the ELF3-PrD) is critically involved in the temperature sensitivity of the EC, as the ELF3 of the Mediterranean grass species *Brachypodium distachyon* has no PrD and does not undergo phase change or accelerated growth at higher temperatures (Jung et al., 2020).

A central feature of ELF3-PrD in *Arabidopsis thaliana* is the presence of a poly-glutamine (polyQ) tract of variable length found to differ in *Arabidopsis* populations by geographic location (Anwer et al., 2014). A similar polyQ tract expansion is responsible for the formation of pathogenic

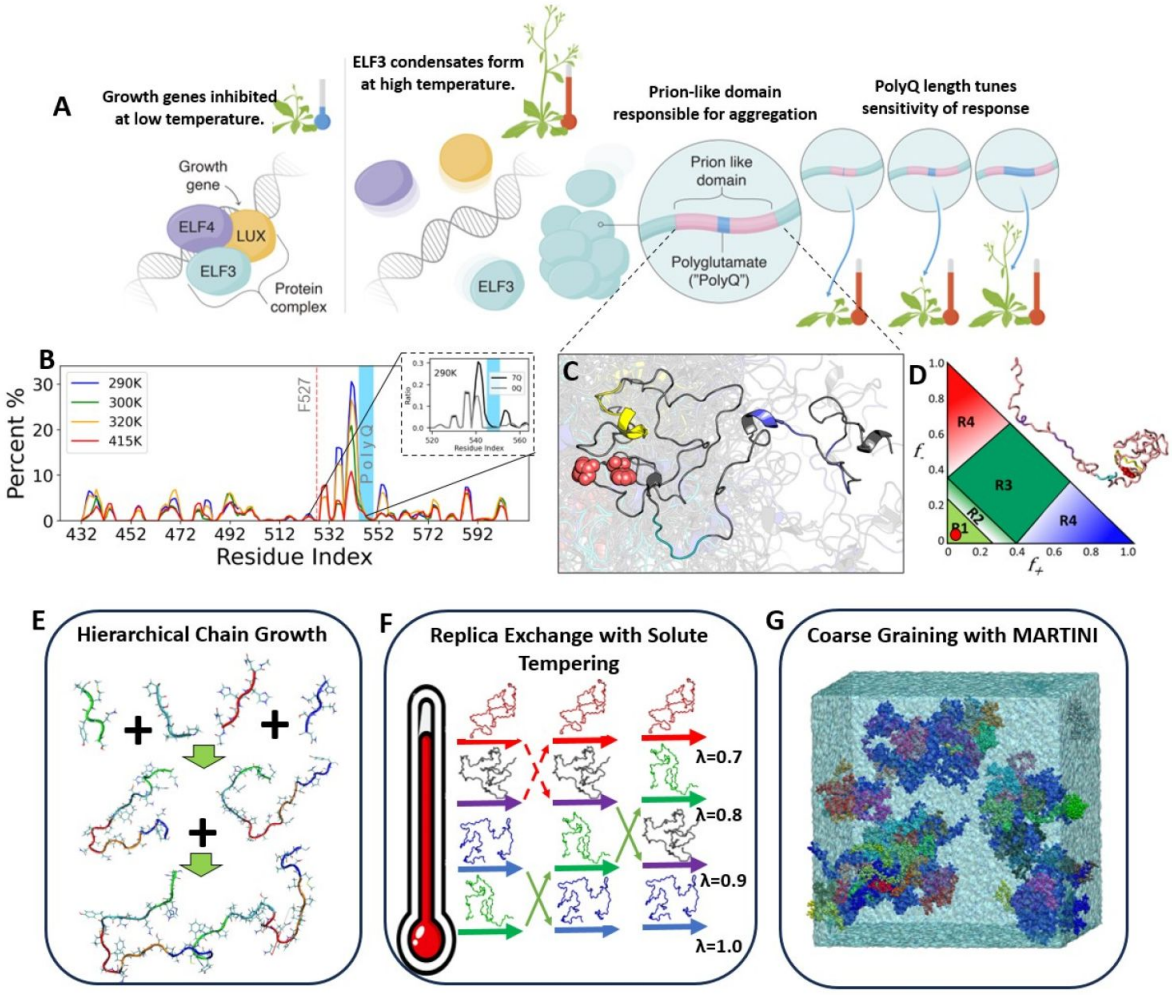

Figure 1.

An overview of the Evening Complex (EC), key features of ELF3, and the computational approaches taken to elucidate the molecular mechanisms of temperature sensing of the ELF3-PrD.

A. An illustration of the temperature-responsive mechanism of the evening complex. The left panel shows the intact EC repressing a growth gene target. Second to left illustrates the complex dissociating from DNA at high temperature. The next section describes the prion-like domain required for condensation and the poly-glutamine region responsible for tuning the sensitivity of the temperature response. The right-most cartoon illustrates the enhanced growth response characteristic of expanded poly-glutamine tracts. **B**. Helical propensity of hierarchical chain growth (HCG) ensembles by residue at four temperatures. The 7Q (wild-type) system is shown in the main panel with a region of interest of 7Q and 0Q shown in the inset. The light blue regions mark the locations of the poly-glutamine tracts and the yellow region highlights an aromatic helix of mechanistic importance. **C**. A structure of wild-type ELF3-PrD taken from a REST2 simulation. **D**. A charge fraction plot commonly used to classify IDPs based on sequence. The red dot indicates ELF3-PrD falls in region 1, classifying it as a weak polyampholite characterized by a globular or 'tadpole-like' shape. **E**. An illustration of the hierarchical chain growth method used to produce ELF3-PrD ensembles at a variety of polyQ lengths and temperature conditions. **F**. A cartoon representation of the REST2 enhanced sampling simulation method. **G**. A snapshot from a coarse-grained Martini simulation used here to investigate temperature-dependent condensation propensity of ELF3-PrD variants.

huntingtin protein aggregates in Huntington's disease patients. However the tract lengths observed in Huntington's disease are longer (>35 residues) than those of ELF3, which contains polyQ tracts of 0 to 29 glutamine residues. (Reiner et al., 2011). Experiments by Jung et al. found the length of this polyQ tract modulates the sensitivity of the temperature response, observing that longer polyQ enhances condensate formation and hypocotyl growth rate at high temperature (Jung et al., 2020). The mechanistic insights gained from studies of ELF3 condensate formation and temperature responsiveness could shed light on general principles governing polyQ-mediated interactions in native cellular contexts.

That evolution has co-opted biological condensates for temperature sensing in *Arabidopsis* aligns with the intrinsic temperature-dependence of condensate formation as well as the nature of IDPs as key sensors of cellular physicochemistry in general (Moses et al., 2023). However understanding the driving forces for IDP condensate formation at high (LCST) vs. low (UCST) temperatures is still just beginning to be understood. Here, condensate formation at higher temperatures, like ELF3-PrD, correspond to those with a lower critical solution temperature (LCST) and those that form condensates at lower temperatures have an upper critical solution temperature (UCST) – these abbreviations will be used from now on. The understanding of LCST vs. UCST behavior has improved recently, for example via sequence heuristics proposed in (Quiroz and Chilkoti, 2015; Ruff et al., 2018), but the understanding physicochemical drivers of native LCSTs is still a work in progress. Sequence heuristics in general are a useful way to understand IDP functions (Maristany et al., 2023), for example they can accurately identify classes of IDP by simply looking at fraction of positive and negative charges in the sequence (**Fig. 1D**) (Das and Pappu, 2013). However, understanding the interplay between the polyQ regions of ELF3-PrD and the other sequence heuristics available is non-trivial. Previous studies have shown that polyQ tracts often enhance helical propensity in adjacent regions (Totzeck et al., 2017), which is of particular interest because short regions of transient helicity called Short Linear Motifs (SLiMs) are often responsible for formation of intra- and inter-protein interactions necessary for biological function (Davey et al., 2012).

The dynamic nature of IDPs has historically complicated their structural characterization (Bari and Prakashchand, 2021; Schramm et al., 2019). Experimental approaches can provide information about ensemble averages, but elucidating information about specific states or clusters of states remains a challenge (Nag et al., 2022). Using computational approaches to bridge this gap and access conformational ensembles, the molecular characterization of condensates is becoming increasingly accessible. While atomistic molecular dynamics (MD) simulations offer the most precise access to these ensembles, the computational cost of sampling the full conformational space of an IDP, not to mention a condensate, is steep. Recent methods for sampling IDPs by decomposing them into their component peptides and sampling these smaller systems individually before stitching them back together has been a fruitful approach in this space (Stelzl et al., 2022; Pietrek et al., 2020; Lindsay et al., 2021). However, this approach is limited, for example, in that it does not explicitly sample long distance interactions. The development of specific forcefields to accurately sample disordered proteins (Best et al., 2014; Song et al., 2017; Robustelli et al., 2018; Wu et al., 2018; Abascal and Vega, 2005) and enhanced sampling methods, like replica exchange with solute tempering (REST2) (Wang et al., 2011a), have also improved the tractibility of atomistic MD simulations of IDPs. However, efficiently computing properties of IDPs, especially on the condensate level, necessitates the use of coarse-grained models, either at the Martini level (Thomasen et al., 2022) or even more coarse grained at the single-bead-per-residue level (Regy et al., 2021; Tesei et al., 2021). Further levels of coarse graining have pushed the possible timescales and system sizes even further with lattice-models (Choi et al., 2019) and even machine-learning algorithms like ALBATROSS and CALVADOS (Lotthammer et al., 2024; Tesei and Lindorff-Larsen, 2022; von Bulow et al., 2024).

In this work, we employ computational techniques to understand how temperature impacts the structural character of the ELF3-PrD ensemble, how polyQ length and sequence context impacts these characteristics, and the impact of each of these factors on dynamics underlying ELF3 condensation. Using a fast and efficient chain-growth algorithm, we produce ensembles of ELF3-PrD at a variety of polyQ length and temperature conditions (**Fig. 1B,1E**). We discover temperature-responsive helices in polyQ-adjacent regions and identify a residue, F527, involved in the temperaturesensing mechanism of the PrD. Next, we employ all-atom replica exchange with solute tempering (REST2) simulations to characterize temperature-sensitive conformation changes that promote condensate formation (**Fig. 1F**). In addition to the wildtype ELF3-PrD, we examine the F527A mutant to characterize the key role played by the F527 residue in the temperature-response mechanism and a 0Q mutant with the variable polyQ tract removed to better understand the role of this polyQ tract in modulating the structural ensemble with increasing temperature. Finally, we perform coarse-grained Martini simulations to more directly study how ELF3-PrD condensation dynamics depend on temperature and polyQ length. Simulating 100 ELF3-PrD monomers in a small box allows us to investigate specific residues that play key roles in driving condensation, including a major role observed for aromatic residues in driving protein-protein interactions underlying condensate formation, while also revealing the impact of sequence context and the expansion or deletion of the variable polyQ tract on the temperature range and sensitivity of the temperatureresponsive phase transition (**Fig. 1G**). Through this computational lens we are able to better understand the role and molecular mechanism of polyQ-adjacent helices and aromatic residues in the temperature-sensitive growth response of *Arabidopsis thaliana* mediated by the ELF3-PrD.

Results

Sequence-based insights on ELF3-PrD properties

Sequence heuristics were already initially useful to identify the existence of the ELF3-PrD (Jung et al., 2020; Lancaster et al., 2014), and further investigation of other heuristics can provide insight into its structural and dynamical properties. One simple first step is to look at the ratio of positive to negative charges in any IDP, which in the case of ELF3-PrD suggests a globular or 'tadpole-like' shape (**Fig. 1D**) (Das and Pappu, 2013). Another simple sequence-level heuristic is the Ω_{aro}, which indicates 'patchiness' of the aromatic residue distribution. For ELF3-PrD this value is high at 0.897, indicating the aromatics are distributed in clusters rather than evenly through the sequence (see Fig. S7 for a visualization of the aromatics within the ELF3-PrD sequence), which is in contrast to other well-known PrD's like FUS that have a bias toward uniformly distributed aromatics (Martin et al., 2020). A further, sequence-based view is that of (Quiroz and Chilkoti, 2015), who demonstrated that repeats of Pro-X_n-Gly were sufficient to provide a generic disordered scaffold that can be tuned to exhibit UCST or LCST characteristic phase separation in designed polymers. Inclusion of polar residues and zwitterionic pairs of charged residues in the X position or adjacent to the Pro-X_n-Gly motifs, where n is ≤ 4, resulted in UCST character while LCST behavior results from the inclusion of nonpolar residues or lysine at these positions (see Fig. S7 for these motifs highlighted within the ELF3-PrD sequence). The X_n component of these motifs is split between non-polar and polar residues with those proximal to aromatic residues being mostly non-polar, suggesting these regions may promote LCST phase separation.

Two sequence-based web utilities to quickly probe the structural features of IDPs are ALBA-TROSS and CALVADOS. ALBATROSS (Lotthammer et al., 2024) is a machine learning-based approach trained on coarse-grained simulations of synthetic disordered IDPs using Mpipi (Joseph et al., 2021b), a coarse-grained force field which emphasizes π-π interactions like those dominant in the dynamics of low-complexity domains (Vernon et al., 2018). CALVADOS (Tesei and Lindorff-Larsen, 2022) predicts structural properties based on an input sequence. However, CALVADOS

does not utilize a deep learning algorithm, but instead runs a coarse-grained simulation in real time using a single bead-per-residue approach in which hydropathy scales inform amino acid interaction strengths. The Flory scaling exponent is calculated by ALBATROSS to be between 0.36 and 0.394 for each variant, slightly above the theoretical value for a collapsed globule, 0.33. This is in agreement with the globular or 'tadpole-like' shape suggested by an earlier heuristic. The radius of gyration (R_g) reported by ALBATROSS is 3.259 nm for 0Q, 7Q, and 19Q, with only the F527A mutant exhibiting a different value of 3.31, suggesting an insensitivity of ALBATROSS to variations in sequence. More structural predictions obtained from ALBATROSS for ELF3-PrD can be found in Table S1. Unlike ALBATROSS, CALVADOS was able to give estimates for values of interest for IDPs at different temperatures, however it estimated the WT Flory scaling exponent, ν, as 0.49, more suggestive of an ideal polymer with little self-interaction and a more extended shape, which is not in line with other methods. CALVADOS predicts a slightly larger R_g value for the WT than ALBATROSS, with the 290K R_g predicted as 3.41 nm. The WT ensemble is predicted to become more expanded at 340K with an $R_g$of 3.73, as is the 13Q variant, shifting from 3.38 nm to 3.73 nm, the 19Q variant, moving from 3.7 nm to 3.8 nm, and the F527A mutant, expanding from an R_g of 3.31 nm to 3.89 nm. Only the 0Q system is not predicted to undergo significant expansion upon heating from 290K to 340K. A comparison of ELF3-PrD R_g values estimated with six different methods can be found in Fig. S8. A complete accounting of CALVADOS predictions for ELF3-PrD can be found in Table S2. While these quick approaches provide initial insights from just the amino acid sequence of any IDP, we found they sacrificed accuracy and precision in their ability to probe the range of environmental conditions relevant to characterize the effect of temperature and polyQ tract length on the conformational landscape of ELF3-PrD.

Chain growth ensembles exhibit helicity in PolyQ-flanking residues

In order to understand how polyQ length and temperature change the behavior of ELF3-PrD, we examined the structural differences between ensembles with varying polyQ tract lengths constructed at different representative temperatures. Using the hierarchical chain growth (HCG) method by (Pietrek et al., 2020), we constructed ensembles of polyQ of 0, 7, 13 and 19 glutamine residues in length each at temperatures of 290K, 300K, 320K and 415K to produce a total of 16 ensembles with 32,000 conformations each, a total of 512,000 structures. For each residue we summed the conformers with α, 3_{10} or π-helix character to obtain a total helical propensity (**Fig. 1B**). We found ELF3-PrD to be composed of short transient helices, with most having helical propensity of only around 5%. Though most of the ELF3-PrD exhibits only light helical character, the helices adjacent to the variable-length polyQ tract had significantly higher propensities, up to 30% for the N-terminal residues and 10% for the C-terminal residues. These regions, which we refer to as putative SLiMs, display some helicity with or without polyQ as seen in the 0Q system, but the polyQ tract seems to increase the portion of the ensemble with helical character (Totzeck et al., 2017). An additional feature of the polyQ-adjacent SLiMs is a degree of temperature-sensitivity not seen elsewhere in the PrD. In the 7Q system, the N-terminal polyQ adjacent SLiM falls from 30% at 290K to 20% at 300K and finally 10% propensity at 415K, while the same region in the 0Q system shows no appreciable reduction in propensity until 415K. The increase in temperature-responsiveness of these SLiMs in 7Q could be a by-product of the higher possible helical propensity enabled by the polyQ tract. Ensembles with polyQ tracts of 13 and 19 residues showed nearly identical results to the 7Q system (Fig. S9). This could be due to a limitation of the 5-residue fragments simulated to build libraries for the HCG method. Overall, it is clear the presence of a polyQ tract has a significant influence on the protein's local structural character and temperature responsiveness.

E-PCA (Lindsay et al., 2018) is a contact analysis method that isolates the top sources of conformational variance (or dynamics when used on MD trajectories) by identifying residue pairs that form and break in a concerted manner. We apply it here to our HCG-generated ELF3-PrD ensembles to identify regions of correlated contacts which may be of mechanistic importance. For each system, the biggest signal consistently comes from three SLiMs directly N-terminally adjacent to the polyQ tract, suggesting correlated contact formation or breaking of contacts in this region

explains most of the conformational variance, at least partially due to helix formation. At 290K, PC1 of all polyQ-containing systems (Fig. S10A, top-left panel, blue) contains a bimodal signal where each peak corresponds to interactions of residues within a polyQ-adjacent SLiM, suggesting some level of communication between these regions. The dominant mode of the 0Q system, on the other hand, exhibits a single peak, indicating communication between these SLiMs plays a less significant role in the contact dynamics of this system. At the maximum temperature, 415K, the contact dynamics of all systems converge, regardless of polyQ presence or length, as evidenced by the nearly identical PC1 values at this temperature (Fig. S10A, top-right panel, red). This peak at the high-temperature condition indicates formation of contacts that comprise the third polyQ N-terminal SLiM. However, one prominent negative value is consistently observed indicating interaction between F527 and Y530 strongly opposes contact formation within this SLiM. The persistence of this signal across ensembles and its location in the region identified as the primary source of conformational variability suggests a potential role for this contact pair in the general mechanism of ELF3-PrD, warranting further study. Further analysis of these chain growth ensembles can be found in the Supplementary Information.

All-atom REST2 simulations reveal temperature-responsive conformation change in ELF3-PrD

While the static conformers generated by the HCG approach provided a relatively quick and resourceinexpensive look at the effects of varying the polyQ tract length and temperature on the local structure of the ELF3-PrD, we turned to a more intensive MD simulation approach to gain a more complete understanding of dynamics underlying ELF3 function. Based on trends seen in the initial HCG results, we decided to run three separate all-atom MD simulations using the REST2 method, including the wild-type ELF3-PrD to obtain a better understanding of the general molecular mechanism underlying temperature-responsiveness, the F527A mutant to understand the contribution of F527 to condensate formation and temperature responsiveness, and the 0Q system to isolate the role of the variable polyQ tract in ELF3-PrD dynamics. As with the HCG ensembles, helical propensity was calculated for all three PrD variants at four separate effective temperatures, 290K, 300K, 320K, and 405K (**Fig. 2A, B** and **C** respectively). Measurements of helical propensity around the variable-length polyQ tract from these trajectories are similar in trend to the HCG ensemble but with significantly larger propensity values, in the range of 30-65% instead of the 10-30%, for the N-terminal adjacent helix (**Fig. 2A**). Additionally, some level of helical enhancement was observed adjacent to all three polyQ tracts of ELF3-PrD rather than only the first as in the HCG case (Totzeck et al., 2017). The second polyQ tract (WT residues 568 to 572) exhibits enhancement in propensity and temperature-responsiveness in its N-terminal SLiM, and the third and last polyQ tract (WT residues 581 to 586) sees minor enhancement in its C-terminal SLiM, increasing to 10% or about double the baseline propensity. This enhancement of helical propensity indicates long-range interactions absent in the HCG ensembles further promote transient structure in the polyQ-flanking residues. The concerted nature of the enhancement of helicity and temperature-responsiveness may be more than a coincidence as enhancement of potential helical propensity could increase the ability to sense temperatures by providing a greater range of signals with more differentiable outcomes. The helical enhancement of polyQ-adjacent regions demonstrates how structural outcomes depend on sequence context, as degree and location of enhancement vary among the three tracts. The impact of sequence is not just local, as is apparent from the structural analysis of the F527A system. Relative to the WT, the F527A mutation attenuates helices, including those around each polyQ tract, despite being 15+ residues from the nearest tract.

While the 0Q system is reported to be significantly less sensitive to changes in temperature, some temperature-responsiveness does remain intact in experiments. The analysis of helical propensity for this trajectory reveals drastic structural deviation due to the absence of the polyQ (**Fig. 5A**), pointing to fundamental differences in the temperature-sensing mechanism compared with WT. In the absence of the variable polyQ tract, a large helix appears between residues 554 and 566 (**Fig.**

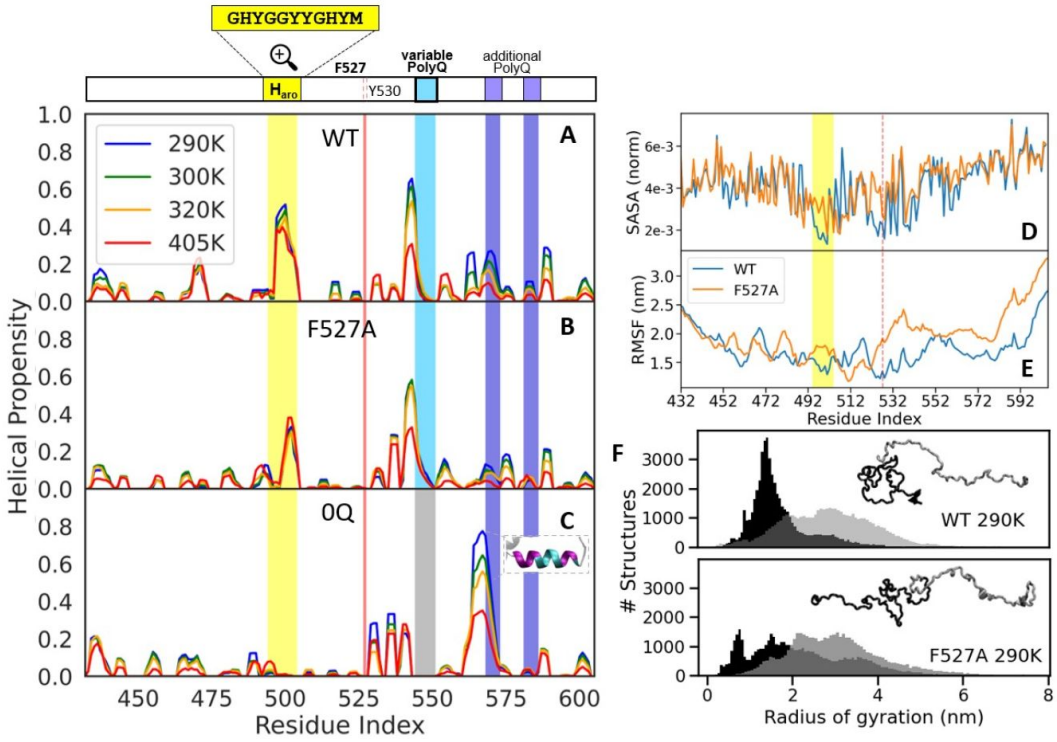

Figure 2.

REST2 simulations reveal local and global conformation changes in response to temperature.

A. Helical propensity of WT REST2 simulation at a range of temperatures. The variable polyQ tract is shaded in blue and the two polyQ tracts of consistent length are shaded in purple. A lengend denoting regions of interest is located at the top. **B**. Helical propensity of F527A REST2 simulation at a range of temperatures. The red line indicates the position of residue 527. **C**. Helical propensity of 0Q REST2 simulation at four temperatures. The gray shaded region indicates the removal of the variable polyQ tract. **D**. Top: Solvent-accessible surface area of WT and F527A systems taken from REST2 trajectories. **E**. The radius of gyration of the first 100 residues (black) and last 73 residues (grey) of ELF3-PrD. Top panel depicts and the WT and the bottom F527A, both at 290K.

2C). This helix exhibits impressive stability at 290K (77% helicity) and rapidly declines linearly as temperature increases, bottoming out at 35% at 405K. This 0Q-native helix includes the first (second in WT) polyQ tract with the bulk of the helix forming N-terminal to polyQ. Aside from formation of this new helix, a distal aromatic helix, discussed further in the next section, is abolished in the 0Q system and helices that were flanking each side of the removed variable polyQ are attenuated. This result indicates the 0Q system may respond to temperature change by a mechanism vastly different from that of the WT, and the location of this new helix is further evidence that polyQ tracts promote helix formation in adjacent residues. Regardless, the interplay of variables like tract length (Totzeck et al., 2017), sequence context (Ramazzotti et al., 2012), tract location, and proximity to other polyQ tracts could all affect protein character and warrant further study.

Aromatics play a major role in temperature-sensitive conformational change

The REST2 simulations painted a more complete picture of the ELF3-PrD dynamics and revealed some mechanistically important features absent in the HCG ensembles, partly due to the inclusion of long-range interactions. The most prominent was a 10-residue helix of heavy aromatic character (residues 494 to 504, "H_{aro}") which was formed between 40-52% of the time in the REST2 WT simulations (**Fig. 2A**) but only present at baseline levels in the HCG ensembles. The F527A mutant sees a significant reduction in the size of this helix (**Fig. 2B**), suggesting long-range interactions with F527 may stabilize H_{aro}. Indeed, it seems this interaction may have consequences for the global conformation of ELF3-PrD. In the WT, both the regions around F527 and H_{aro} are largely buried, as shown by the low solvent-accessible surface area (SASA) in **Fig. 2D**, and their relative immobility as exhibited by RMSF values shown in **Fig. 2E**. A methionine residue of H_{aro}, M504, promotes compaction of this region through interaction of the sulfur atom with the ring of multiple local aromatic (tyrosine) residues (Fig. S11), a common but often overlooked motif (Valley et al., 2012). Upon mutation of F527 to alanine, both the F527 and H_{aro} regions become relatively solvent-exposed and flexible. This interaction influences the global shape of the protein by pushing the N-terminal region towards a globular conformation while the C-terminal region remains relatively extended. This is demonstrated by comparing the $\boldsymbol{R}_g$ of the first 100 and last 73 residues for the WT and mutant systems, as in **Fig. 2F**. The first 100 residues of the WT (top panel) have a sharp peak indicating a compactness not observed in the mutant (bottom panel) while the last 73 residues sample a wide range of $\boldsymbol{R}_g$ values in each case, indicating a more expanded and flexible nature. The mean $\boldsymbol{R}_g$ of the whole PrD for the WT 290K ensemble is 2.75 nm, significantly more compact than predicted by heuristic models ALBATROSS and CALVADOS which reported values of 3.26 nm and 3.41 nm, respectively, as shown in Fig. S8.

Upon discovering the global structural influence of the long-range interaction between F527 and H_{aro}, we set out to determine its role in temperature-responsiveness. The minimum distances between atoms of F527 and H_{aro} were examined under different temperature conditions, and we found a linear increase in F527 and H_{aro} distance (and decrease in interaction) with increasing temperature, as demonstrated by the histograms in **Fig. 3A**. To get a better sense for the role of this temperature-responsive property in the conformational landscape of the protein, we plotted the F527-H_{aro} distance vs the radius of gyration in **Fig. 3B**. At 290K, the WT is largely homogeneous, mostly constrained to a single population of tightly interacting F527-H_{aro} and compact structures. However, with increasing temperature the ensemble shifts towards a second population that is slightly expanded with the F527-H_{aro} contacts broken. Representative structures of the low-temperature and emergent high-temperature populations are depicted in **Fig. 3A** on the left and right, respectively. The F527A mutant reinforces the importance of F527 in the WT conformational landscape as F527A samples a diverse range of populations in this space. However, the most persistent F527A population has significant overlap with the WT high temperature population, suggesting the F527A mutant may mimic the phenotype of WT ELF3-PrD

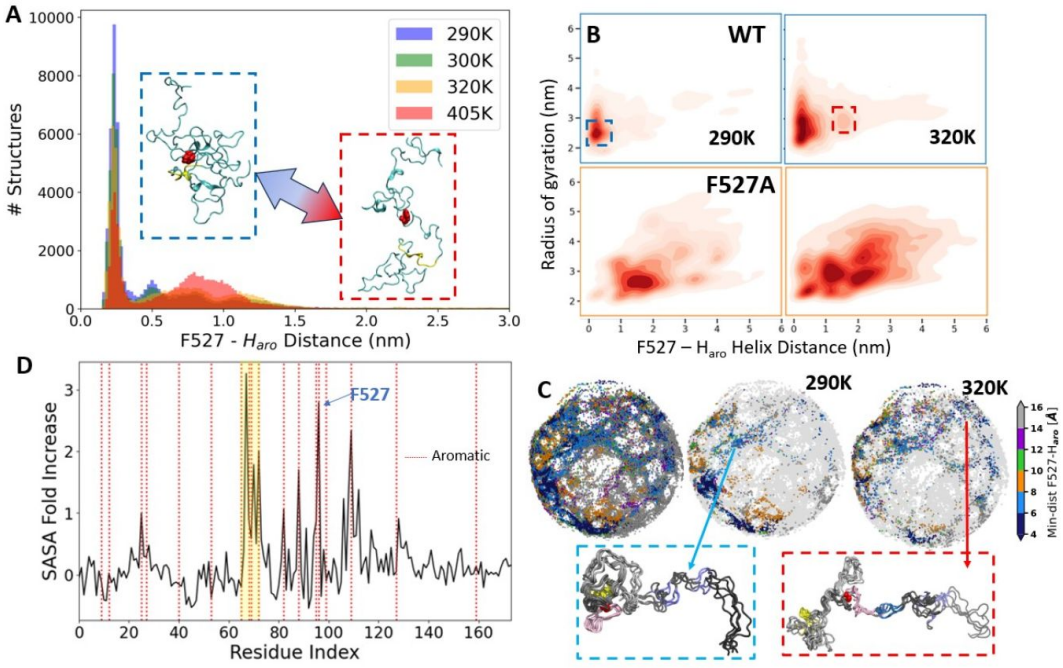

Figure 3.

Temperature-responsive breaking of aromatic interactions exposes sticky aromatic residues to the solvent.

A. The minimum distance between residue F527 and H_{aro} is plotted by temperature from the WT REST2 simulation. Representative low and high temperature structures are inside of a dashed blue or red box, respectively. F527 is in red and H_{aro} is in yellow. **B**. Free energy landscapes of WT (left) and F527A (right) with the X-axis defined as the minimum distance between residue 527 and H_{aro} and the y-axis defined as the radius of gyration. Each ensemble is represented at 290K and 320K. The blue box is the most populated region of conformation space at low temperature and the red box demarcates the emergent high temperature cluster. **C**. ELViM plots illustrating the conformation space of the full ensemble (left), the 290K ensemble (middle) and the 320K ensemble (right) where the color of each dot represents the minimum distance between F527 and H_{aro}. Below are example clusters of conformers with the left representing a commonly populated area at low temperature and to the right a cluster only observed at increased temperature. **D**. Fold increase in SASA between the identified low- and high-temperature populations. Dotted red lines represent aromatic residues and the yellow-shaded region are residues of H_{aro}.

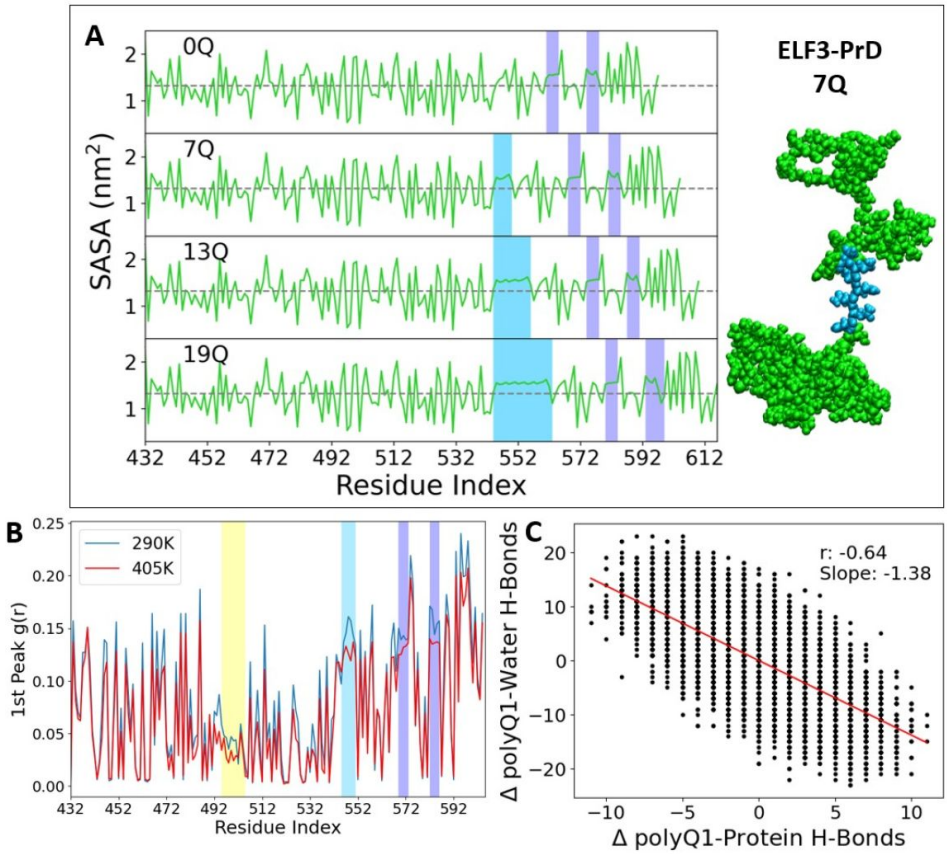

Figure 4.

Cluster formation and monomer conformation change are driven by similar aromatic residues.

A. The solvent-accessible surface area is shown for each HCG polyQ condition at 290K. The variable polyQ tract is highlighted in sky blue and the second and third polyQ tracts in a lighter blue. The black dashed line demarcates the average SASA value for the system. **B**. Per-residue hydration plot of ELF3-PrD WT at 290K (blue) and 405K (red). Each value represents the maximum height of the first peak of an RDF between the given residue and solvent oxygen atoms. The aromatic helix, H_{aro}, is highlighted in yellow and the polyQ tracts in sky blue. **C**. A scatter plot relating change in hydrogen bonds between the variable polyQ tract and water with the change in hydrogen bonds between polyQ and protein from the wild-type REST2 simulation at 290K. Breaking of polyQ-water hydrogen bonds is correlated with an increase in polyQ-protein bonds.

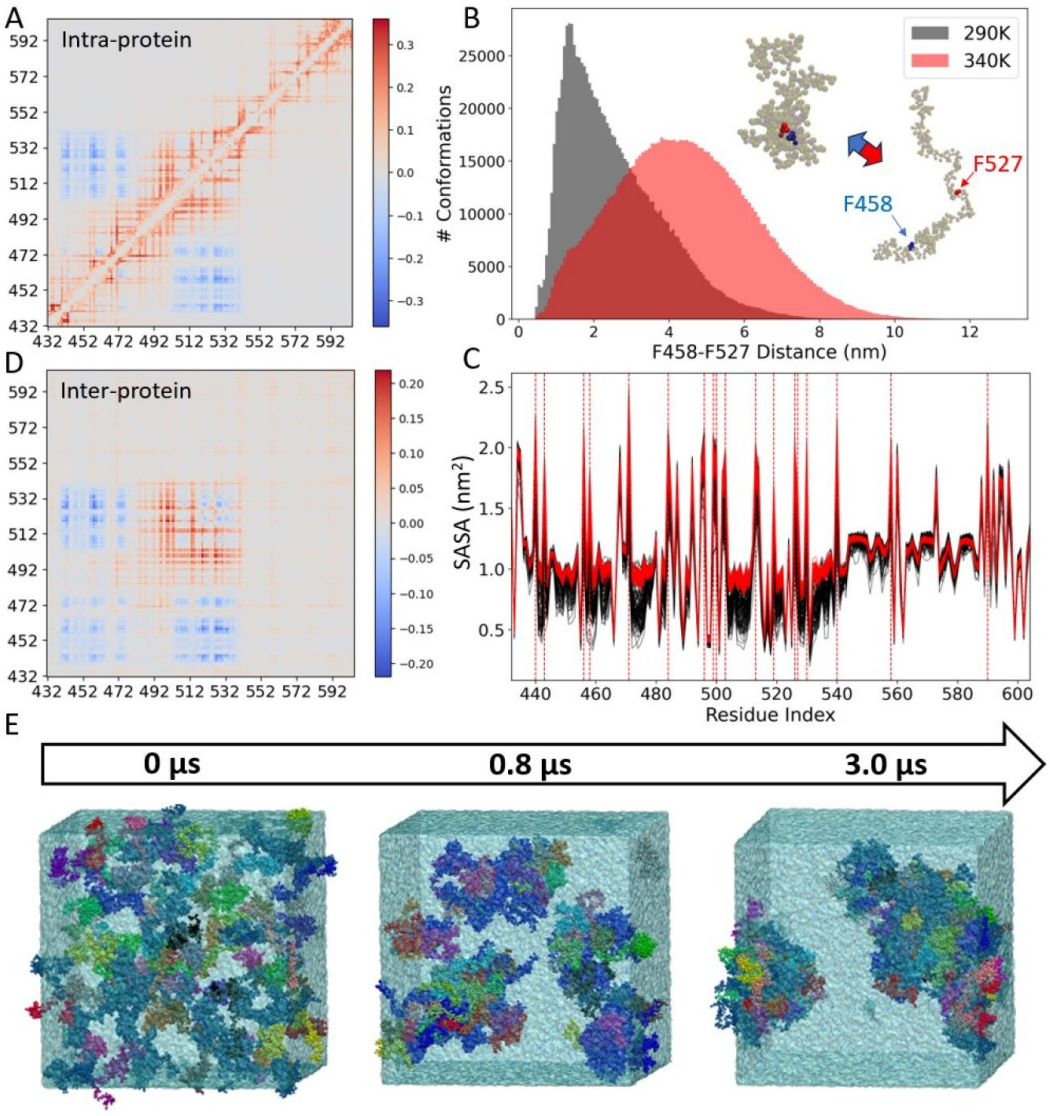

Figure 5.

Temperature-dependent conformation change enhances SASA of CG monomers and promotes cluster formation driven by central aromatic residues.

A. The intra-protein contact difference map between the 340K and 290K WT Martini condensate simulations. Values in red represent increases in contact value at 340K relative to 290K and blue represents a decrease. The entire 3 μs trajectories were used to create these difference maps.**B**. Distance distributions between residue F527 and F458 at 290K (grey) and 340K (red) from WT CG condensate simulations. Distances are taken from intra-protein distances of each monomer. **C**. The solvent accessible surface area is plotted for all 100 monomers of both the 290K WT condensate simulation (black) and the 340K WT condensate simulation (red). **D**. The inter-protein contact difference map between the 340K and 290K WT Martini condensate simulations. As with **Fig. 5A**, contacts enhanced at high temperature are in red with those broken in blue. **E**. An illustration of the typical time evolution of an ELF3-PrD condensate simulation at 300K with simulation snapshots representing approximately 0 ns, 800 ns, and 3μs, respectively.

at high temperatures. In **Fig. 3C**, we've employed the ELViM method (Viegas et al., 2024) to project the WT and F527A conformations onto a common space, where each conformer is a dot colored by the minimum distance between F527 and H_{aro} value. The projections on the left of **Fig. 3C** represent conformers from all four temperature conditions while those to the right represent specific temperature conditions. These projections further demonstrate the degree to which the F527A mutant alters the conformations sampled by ELF3-PrD and illustrates how increasing the temperature from 290K to 320K promotes access of the WT to new regions of conformational space. Additional visualizations and analysis of the ELF3-PrD conformation space can be found in the SI. Interestingly, in the 0Q system, the F527-H_{aro} interaction losses this temperature-responsiveness (Fig. S12) at all but the highest temperatures where we actually see an increase in the interaction propensity. This along with the 0Q-specific temperature-responsive helix suggest a different temperature-sensing mechanism in absence of the variable polyQ tract.

The temperature-dependent breaking of the F527/H_{aro} interaction is particularly interesting due to its potential relevance to ELF3-PrD condensate formation. A significant increase in total SASA is observed in the high-temperature population with a major source being aromatic residues (Fig. S13). As previously mentioned, H_{aro} and F527 are regions of enhanced aromatic residue density, as seen from the dashed red lines in **Fig. 3D**. Breaking the interaction between F527/H_{aro} frees up 5 aromatic residues from these regions (Y496, Y499, Y500, Y503 & F527) and as well as four aromatic residues located between F527 and H_{aro} which can become buried during their interaction. Indeed, our high-temperature population exhibits enhanced solvent accessible surface area for these residues and for the majority of the 18 aromatic amino acids present in the ELF3-PrD with those residues located between H_{aro} and F527 especially affected (**Fig. 3D**). Given the wellestablished role of aromatic residues in driving interactions in low complexity disordered protein regions (***Martin and Mittag, 2018a***), it is reasonable to expect an increase in condensate formation propensity when these residues are accessible by other ELF3-PrD monomers. Indeed, previous work has established a link between single-chain dimensions and phase-separation propensity as a function of aromatic character (Dignon et al., 2018; Martin et al., 2020).

PolyQ solvation dynamics contribute to ELF3-PrD condensate forming propensity

A key question to understand temperature sensing by ELF3 is how expansion of the polyQ tract enhances the phase-separation propensity of ELF3-PrD, thus increasing the temperature sensitivity of condensation (Jung et al., 2020). One potential driver is the increasing availability of glutamine on the protein surface with increasing tract length. Plotting the SASA values for our HCG ensembles (**Fig. 4A**) highlights all three polyQ tracts as regions of persistent high solvent accessibility. While the SASA value of polyQ tracts is only moderately higher per residue than the average, indicated by a dashed black line, it persists for the length of the tract, creating patches of high solvent accessibility not seen elsewhere in the PrD. SASA values for these HCG ensembles were temperature-invariant for each case. Similar to the effect of increasing temperature in our REST2 simulations, increasing polyQ length enhances the overall solvent accessibility of the protein. PolyQ tract expansion provides a direct and tunable means to enhance PrD solvent-accessibility.

Solvation dynamics serve as a determining factor in condensate formation behavior, in part by determining which regions remain accessible to the solvent and other proteins, and changes in temperature can alter these dynamics. To characterize how hydration differs across ELF3-PrD we obtained radial distribution functions (RDFs) of water oxygen atoms around ELF3-PrD as a whole and around each individual residue. Values for a per-residue solvation plot were obtained by using each residue as the reference point for an RDF calculation of water oxygen atoms and plotting the height of the first peak, representing the most tightly bound water molecules, referred to as the first solvation shell (**Fig. 4B**). At 405K, many residues exhibit a decrease in local solvation, with the most prominent and continuous decreases seen in the three polyQ tracts.

Further investigation of ELF3-PrD polyQ interactions at high temperature show a tradeoff wherein a decrease in polyQ-water hydrogen bonding is compensated by an increase in protein-protein hydrogen bonds, even though the number of polyQ-proximal water molecules increases (**Fig. 4C**). This is consistent with studies that have suggested water is a poor solvent for glutamine (Khare et al., 2005). This characteristic may influence condensation, either by promoting polyQ-protein interactions or altering the solubility of the protein.

PolyQ tract length modulates temperature-responsiveness of PrD clustering

We next shift our focus from the structural ensembles of ELF3-PrD monomers to the condensation dynamics of the system. Performing coarse-grained Martini simulations provides a more direct way to identify interactions which drive protein-protein interactions of the PrD and to observe the ways in which variables like polyQ tract length and sequence mutations modulate the formation and stability of clusters in response to temperature. We first examine the impact of temperature on contact dynamics of the 100 monomers that comprise our condensate simulations to see how they align with our all-atom simulations. The contact difference map seen in **Fig. 5A** provides an understanding of how intra-protein interactions change with increasing temperature. The blue regions indicate interactions between an N-terminal region of the PrD with centrally located aromatics at 290K which are broken at 340K. Corresponding red lines in the central region indicate an enhancement of local interactions between aromatic residues within this region. This breaking of long-range contacts at increased temperature is similar to the temperature-induced conformational shift observed in the all-atom simulations. Here, F527 interacts in a temperature-dependent manner with F458 instead of the H_{aro} region (**Fig. 5B**), as was observed in the REST2 simulations. These Martini simulations do not capture transient helices, which may account for the lack of interaction with H_{aro}, but the trend is very similar nonetheless. By plotting the per-residue SASA of each of the 100 PrD monomers in **Fig. 5C**, a clear increase is seen across all residues, with the biggest peaks aligning with the aromatic residues. Based on a similar observation in the all-atom systems, we inferred that these residues would participate in inter-protein interactions, however, here we can observe these interactions directly. The inter-protein contact difference map in **Fig. 5D** indicate an increase in interaction between centrally-located aromatics at 340K as compared to 290K. An illustration of a WT PrD cluster forming at increased temperature is seen in **Fig. 5E**. The intra- and inter-protein difference maps are strikingly similar, suggesting the same interactions are responsible for monomer dynamics drive protein-protein interactions. We further explore the intra-protein interaction propensities of the aromatic residues in Fig. S14 which demonstrates the degree to which interactions between aromatic residues control the dynamics of this low complexity domain. The overall shape of the interaction profiles are nearly identical with only their scales varying, suggestive of the universal nature of aromatic contacts in these types of proteins. This plot provides some insight into the similarities observed in the intra- and inter-protein contact maps.

Our coarse-grained simulations allow us to measure the temperature dependence of ELF3-PrD clustering and how polyQ length and sequence mutations impact size and stability of clusters. Following the procedure used by previous protein condensate studies, we track the number of monomers comprising the largest cluster as a proxy for condensation propensity (Benayad et al., 2021; Joseph et al., 2021a). Cluster membership is determined using a cutoff of 0.5nm between backbone beads of individual monomers. The convergence of 100 ELF3-PrD monomers into a few large clusters is illustrated for each of these conditions at 290K in **Fig. 6A** with conformers taken from a wild type simulation at around the 0, 1 and 3 μs. We take a closer look at the temperature dependence of cluster formation for the wild-type system in **Fig. 6B**. Here, there is a clear increase in maximum cluster size given a temperature increase from 290K to 300K. This represents a biologically relevant temperature range and is close to the temperatures used in experiments (Jung et al., 2020). Clustering occurs more slowly at 320K and only briefly reaches the size seen at 300K before the end of the 3 μs simulation, but is still enhanced relative to 290K. At

340K clustering no longer occurs on a large scale with the largest clusters being around 10 monomers in size and transient in nature. We can gain insights into the driving force of temperature-dependent condensation by examining the net change in total contacts per residue of the 7Q system at 300K vs. 290K during the last microsecond of simulation, when the clusters are most fully formed (**Fig. 6C**). While an increase in contacts is observed for every residue at 300K, aromatic residues exhibit dramatic gains, clearly visible as large spikes in the net contact plot. As clusters start to form, the polyQ tract expels water molecules in exchange for increasing polyQ-protein interactions, as shown for the 7Q system at 300K in **Fig. 6D**.

Expansion of the polyQ tract to 19Q (Fig. S15) results in similar trends seen in the wild type at 290K at 300K, with enhancement of clustering observed at 300K resulting in clusters moderately larger than those exhibited by the wild type. At 320K, the 19Q system exhibits no enhancement of clustering compared with the 290K condition, revealing a difference between the 19Q and 7Q systems. Cluster formation is not observed at 340K, a trend seen in each ELF3-PrD variant simulated here. Interestingly, the variable polyQ tract of the 19Q system exhibits fewer protein-water interactions than the WT when normalized by tract length (Fig. S16). Removal of the variable polyQ tract, as in the 0Q system (Fig. S17), results in smaller clusters in the 290K condition compared with wild type. Enhancement is again observed at 300K, but now the 320K condition exhibits an increase of cluster formation on par with that at 300K. These results indicate polyQ expansion enhances the condensation of ELF3-PrD in the biologically relevant temperature range of 290K to 300K and removal of the polyQ tract does not result in an inability to form clusters, but reduces the condensation at 290K while maintaining stability at a higher temperature of 320K when compared 7Q and 19Q.

In addition to polyQ length, we performed a set of simulations probing the dynamics of cluster formation of the F527A mutant in response to temperature (Fig. S18). As with the polyQ variants, an increase in maximum cluster size is observed at 300K as compared with 290K. However, a marked decrease in cluster size is observed at 320K. This data suggests a more narrow range of effective clustering temperatures for the F527 mutant compared with the 7Q wild type system. These simulations suggest removal of one of the key drivers of protein-protein contacts, F527, narrows the range of temperatures at which clusters are stable and conducive to liquid-liquid phase separation. Due to its prominent role in temperature-responsive conformation change, we expected that F527A mutant would result in more expanded condensation-prone conformations, however, removal of F527 eliminates one of the key drivers of protein-protein interaction. This impedes to the ability of the F527A ELF3-PrD mutant to form stable condensates and reinforces the importance of sequence context in condensation of low-complexity domains.

Discussion

We have used varying levels of simulation accuracy to understand the molecular basis for the ELF3-PrD-based temperature response in plants. Together, these methods have enabled us to propose mechanisms by which ELF3-PrD responds to temperature to promote protein-protein interaction and condensation. Initial sequence-based methods allowed us to put the ELF3-PrD in the context of other IDPs: a ‘tadpole’-like weak poly-ampholite (Mao et al., 2010) with some sequence characteristics in line with those seen for other LCST proteins (Martin and Mittag, 2018b; Dignon et al., 2019). Furthermore CALVADOS indicated some temperature dependent changes in radius of gyration, but CALVADOS and ALBATROSS gave different results for values like the Flory scaling exponent. However, we sought a more molecular-level understanding of the temperature-dependent properties of this process by building HCG ensembles at different temperatures and with different polyQ lengths to find that the variable polyQ was flanked by temperature-sensitive helices. These initial HCG results also indicated the importance of aromatic residues – specifically the F527. Extensive molecular simulations with REST2 allowed us to observe the temperature-dependent conformation landscape of the ELF3-PrD, including crucial long-range

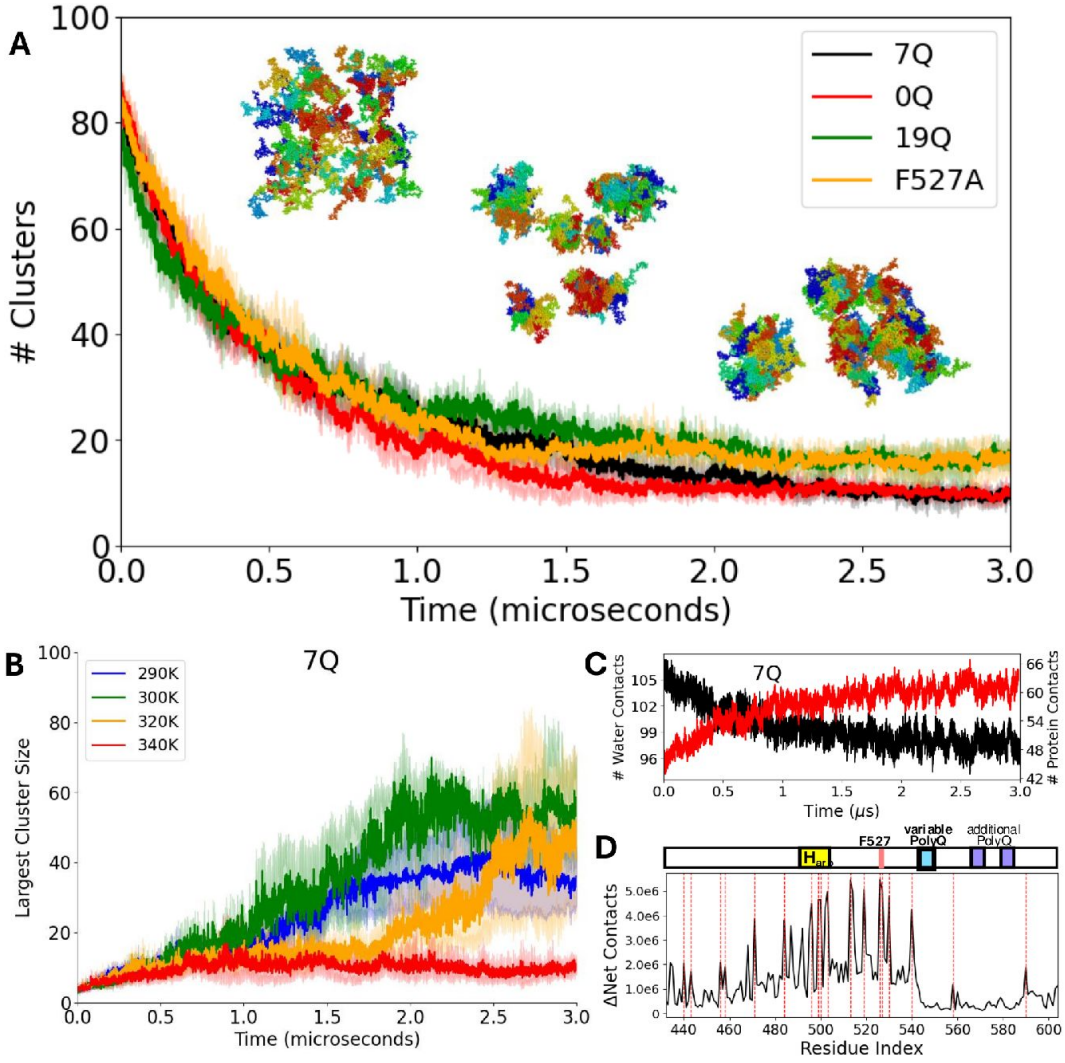

Figure 6.

Martini 3 simulations capture the temperature of condensate formation of ELF3-PrD.

A. The number of ELF3-PrD clusters over time for the 7Q, 0Q, 19Q and F527A systems at 290K is illustrated with standard deviation. A cluster is defined using a 0.5nm cutoff between backbone beads. **B**. The number of ELF3-PrD monomers in the largest cluster from the wild-type simulations at four different temperatures. **C**. The number of water molecules interacting with the variable polyQ tract is demonstrated for 7Q at 300K in black. The concurrent number of protein interactions with the variable polyQ tract is shown in red. **D**. The net difference in protein contacts per residue at 300K vs 290K is plotted for the wild type ELF3PrD. Aromatic residues are denoted by dashed red lines.

aromatic interactions not captured by HCG, like that of F527 and H_{aro}. Note that with an initial preprint the HCG and REST2 data of the atomistic ELF3-PrD simulations were made public at an early stage, and several groups analyzed these terabytes of data to test their methods, and found similar corroborating analyses to those presented here (Viegas et al., 2024; González-Delgado et al., 2024). Finally, coarse-grained Martini simulations showed that the expansion of the variable polyQ tract from 7Q to 19Q enhances condensate formation at the biologically relevant temperature of 300K, while the 0Q variant demonstrated smaller clusters at 290K and increased stability at 320K, potentially indicating an increase in the critical temperature required for phase separation. Additionally, the F527A mutant exhibited a decrease in cluster stability above 300K relative to the other variants studied, likely due to the removal of an important 'sticker' residue. These CG simulations further highlighted the importance of the aromatic residues for condensate formation, especially a central aromatic cluster with marked changes in contacts at different temperatures.

Overall, this molecular approach has helped understand the interplay of the varied sequence contexts of the ELF3-PrD and how they effect transient structures and temperature dependence. Here we found that aromatic residues, especially F527 and the central aromatic cluster, are key to condensate formation for this IDP, consistent with other analyses of condensate-forming IDPs (Martin et al., 2020). Furthermore, the transient temperature-dependent helices flanking the polyQ's points to the importance of the sequence context around the polyQ's. It is possible it is exactly this context that has reinforced these domains and the plasticity of polyQ motifs for adaptive temperature sensing, even when excessive polyQ length leads to disease (Reiner et al., 2011). These transient helices are reminiscent of SLiMs found in other IDP systems (Davey et al., 2012).While SLiMs have been seen to play a role in condensate formation, for example in TDP43, here we see a decrease in helicity as temperature increases, so this SLiM formation anti-correlates with condensate formation. The breakdown of these transient helices at high temperatures exposes aromatic residues to enhance condensate formation at higher temperatures (Fig. S22). Furthermore, a possible role for these putative SLiMS around the polyQ motifs is to enhance protein-protein and protein-DNA interaction with the rest of the EC complex at lower temperatures, when they are more stable.

Understanding the role of these transient helices in condensate formation from molecular simulation is complicated by the pros and cons of the various simulation methods used. The HCG and REST2 simulation both consistently found these polyQ-adjacent temperature-dependent helices, actually more prominent in the more accurate REST2 simulations (though we acknowledge reports of REST2 sampling overly compact states (Zhang and Chen, 2022)). These helices, however, are not well-captured in the coarse-grained simulations necessary to simulate condensate formation, as the only option is to explicitly enforce them with an elastic network model. However, we believe that the overall properties of these coarse-grained simulations are encouraging, as the contact maps and radius of gyration were overall very similar to those seen in the REST2 simulations. Furthermore, that Martini 3 was able to show increase in condensate-forming propensity at higher temperatures for the WT ELF3-PrD and an increase in condensate-forming propensity for a longer polyQ tract is encouraging for the relevance of this force-field for studying LCST systems. For example, our attempts at using other single-residue-per-bead forcefields with implicit solvent like HPS (Dignon et al., 2019) lead to much more compact conformations than we observed in atomistic simulation (Fig. S19), and especially noting the importance of protein-water interactions for LCST systems, we chose to not go this route.

The importance of understanding the ELF3-PrD temperature sensing mechanism in plants has increased since its original discovery (Jung et al., 2020) as more similar systems have been described (Zhao et al., 2017; Bohn et al., 2024), and the threats of a warming planet on plant and crop health have become ever clearer. The results we present here help elucidate some of the molecular origins of this temperature sensitivity, however it is clear there is much work still to do. For example the simplified system we have studied here of the 173 residue ELF-PrD without the

rest of the 695 residue protein and in the absence of the members of the EC (LUX, ELF4, and DNA) begs for further studies within a more realistic context, though ELF3-PrD condensate formation has been seen *in vitro*. Relatedly, both *in vitro* and *in vivo* experimental validation of the molecular mechanisms we postulate is an essential path forward. Overall, though, we believe that this study has taken the cutting edge of computational capabilities in the field of biomolecular condensate toward understanding a biologically important LCST.

Methods

Hierarchical Chain Growth Method and Simulation Details

The sequence for *Arabidopsis thaliana* ELF3 was obtained from UniProt. The PrD sequence (residues 432 to 604) was isolated and divided into 57 segments. Each segment was five amino acids in length including two residues that overlap with the previous segment and two residues that overlap with the subsequent segment. Each of the 57 segments was capped with an N-terminal acetyl group and a C-terminal N-methyl group to neutralize interactions of the charged ends of the protein. Segments were parametrized using the Amber03ws forcefield (Best et al., 2014) and placed in a periodic rectangular box with 1nm of padding on each side of the protein and solvated with TIP4p2005 water molecules (Abascal and Vega, 2005).

Each segment was minimized until the maximum force reduction dropped below 1000 kJ/mol/nm per minimization step. For each of the 57 segments, 24 replicates were equilibrated to various temperatures ranging from 290K to 405K for 10ns. For this step, temperature effects were implemented using the v-rescale thermostat and the Berendsen barostat (Berendsen et al., 1984).

Finally, replica exchange MD was run for each segment for 100ns using GROMACS version 2021.1 (Abraham et al., 2015). For this production run, the v-rescale thermostat was used to maintain temperature and the Parrinello-Rahman barostat (Parrinello and Rahman, 1980) was used to maintain a pressure of 1 bar.

Once the fragment simulations were finished, we used the hierarchical chain growth (HCG) application, developed by Pietrek *et al*., to construct a 7Q ELF3-PrD ensemble from these 57 segments consisting of 32,000 unique conformations (Pietrek et al., 2020; Stelzl et al., 2022). Conformers were randomly chosen from each segment and joined in a pairwise fashion to create a set of fragment dimers. These were then joined into tetramers, octamers, and so on until the full 57-segment ELF3-PrD was reconstructed. This process was repeated until we had obtained ensembles with polyQ tracts of 0, 7, 13 and 19 residues in length each at temperatures of 290K, 300K, 320K and 415K for a total of 16 ensembles. Due to the two-residue overlap, we were required to run 19 segments made up of residues C-terminal to the polyQ region in order build the 0Q, 13Q and 19Q systems.

REST2 Simulation Details

The HCG method enabled us to quickly look at large ensembles of different polyQ conditions for potential structural differences and pointed us towards some regions and residues of interest. The usefulness of the HCG method, for our purposes, is limited by the absence of long-range interactions. In order to accurately study the dynamics of ELF3-PrD we turn to REST2 (Replica Exchange with Solute Tempering), an all-atom enhanced sampling technique capable of exploring longer effective time scales than traditional all-atom MD (Jo and Jiang, 2015). Much like temperature replica exchange (T-REMD), REST2 runs multiple replicas in parallel, each at a different effective temperature. Every few hundred MD steps, replicas attempt to swap with one another with the probability of acceptance tied to the energy difference between replicates (Wang et al., 2011b). Unlike T-REMD where temperatures values are set for each replica, REST2

modulates the strength of protein-protein and protein-water interactions to achieve an effective temperature, a feature which reduces the number of replicas required compared with T-REMD. While REST2 can still be resource intensive, it is one of few methods able to provide Boltzmann-distributed ensembles of IDPs at biologically relevant timescales.

REST2 simulations (Wang et al., 2011b) were performed of the full-length wild-type ELF3-PrD, the ELF3-PrD F527A mutant and the 0Q ELF3-PrD with the variable polyQ tract removed. For the initial structure of these simulations, we chose an especially helical conformer from our HCG wildtype ensemble created at 290K. For the F527A mutant, F527 was manually edited to alanine by removing side-chain atoms and changing the residue name in the structure file. Each system was inserted into a rectangular periodic box with 1 nm of padding around each side of the protein and treated with the Amber03ws forcefield (Best et al., 2014) and the TIP4p2005 water model (Abascal and Vega, 2005). The wild-type system contained 2606 protein atoms, 122623 TIP4P water molecules, 439 Na atoms and 342 Cl atoms for a total of 490489 atoms. The F527A mutant matched this setup but with 2596 protein atoms for a total of 493769 atoms. The 0Q system contained 2487 protein atoms, 210607 water molecules, 237 Na atoms and 240 Cl atoms for a total of 846088 atoms. A 50ns equilibration run was performed for each system using the v-rescale thermostat and Berendsen barostat (Berendsen et al., 1984). After equilibration, each protein atom was marked within the base topology file as a "hot atom" and replicas were created by scaling interactions involving these "hot atoms" by a lambda value corresponding to temperatures in the range of 290K to 405K. The wild-type and F527A systems each had 20 replicas while 0Q had 12 replicas in order to achieve an exchange probability between 35% and 45%. REST2 production runs of each system were performed for 500ns using the v-rescale thermostat and Parrinello-Rahman barostat (Parrinello and Rahman, 1980). Convergence was verified using a split analysis of the radius of gyration values for each system at multiple temperatures (Fig. S20).

Martini Simulation Details

All condensate simulations contain 100 ELF3-PrD monomers in a 40 nm^3 box. Monomers used for the initial configurations were obtained by performing an RMSD-based cluster analysis on previously run all-atom REST2 simulations of ELF3-PrD monomer. A representative structure was taken from 10 of the most populated clusters and each was converted to Martini format using Martini 3.0 and inserted into the box 10 times for a total of 100 monomers. Protein-water interactions were scaled up by 10%, a procedure shown to bring simulated proteins into better agreement with experimental measurements (Thomasen et al., 2022). Each initial configuration was equilibrated for 50ns to four different temperatures, 290K, 300K, 320K and 340K followed by production runs of 3 μs. This process was performed for wildtype (7Q), 0Q, and 19Q ELF3-PrD, as well as the F527A mutant. All systems used explicit Martini water and contained 150mM NaCl. Three replicates were performed for each condition with the exception of wild type and F527A at 300K and 19Q at 340K, which have two replicates each.

Statistical Analysis of Ensemble Contact Maps

We used two types of contact analysis to identify mechanistically important interactions and characterize differences in our ELF3-PrD chain-growth ensembles. Both approaches, E-PCA and I-PCA (Johnson et al., 2018), are part of the CAMERRA family of contact analyses developed by Shen *et al.* and seek to explain sources of conformational variance of protein ensembles. In E-PCA, contact maps from each conformation of the ensemble are used to produce a contact covariance matrix of each possible residue pair, *i* and *j*, with all other residue pairs, *k* and *l*. PCA is performed using this covariance matrix as input and the top PCs are returned. This method has been used to uncover coordinated interactions underlying mechanisms of allostery, cooperative ligand binding, and general collective motions of a variety of proteins (Lindsay et al., 2018; Clark et al., 2016; Johnson et al., 2015a,b). Due to the absence of long-range interactions in the HCG method used to generate our ensembles, E-PCA signals will be more prominent for local interactions. The

dynamics of folded proteins tend to be dominated by the top few modes (PCs), however, intrinsically disordered proteins exhibit a slower eigen decay in which the first several PCs may contribute nearly equally (Fig. S21).

The second CAMERRA variant, I-PCA, provides information on the packing of residues and can identify regions of the sequence in which residues tend to interact more frequently. In this approach, individual residue pairs are considered against the rest of the protein, resulting in a covariance matrix of size $N \times N$ as opposed to $N^2 \times N^2$ for the E-PCA variant. This approach has been prominently used in studies of chromatin structure to differentiate transcriptionally active and inactive regions (euchromatin and heterochromatin, respectively) from Hi-C maps (Lajoie et al., 2015). When applied to natively structured proteins I-PCA tends to identify the individual domains of the protein and while IDPs do not contain structured domains, I-PCA can nevertheless identify dynamically associated domains (Lindsay et al., 2021).

Acknowledgements

We would like to acknowledge Lucy Reading-Ikkanda for providing the illustrations in **Fig. 1A**, Lukas Stelzl and Lisa Pietrek for developing the hierarchical chain growth method used here, and Javier González Delgado and Juan Cortes for characterizing the conformational landscape of the ELF3 REST2 simulations using their WARIO contact analysis method and subsequent discussions. VBPL is supported by the Brazilian agencies FAPESP (Grants 2023/02219-1 and 2022/07231-7) and National Council for Scientific and Technological Development – CNPq (Grant 310017/2020-3).

Data Availability

The datasets generated and analyzed during the current study are available for download: HCG ensembles: *https://users.flatironinstitute.org/~ccb/smbp/elf3_data/elf3prd_hcg.zip* REST2 trajectories: *https://zenodo.org/doi/10.5281/zenodo.13226984* Martini trajectories: *https://zenodo.org/doi/10.5281/zenodo.13285376* Analysis scripts and code: *https://github.com/flatironinstitute/ELF3*

References

Abascal JLF, Vega C. (2005) **A general purpose model for the condensed phases of water: TIP4P/2005** *The Journal of Chemical Physics* **123** https://doi.org/10.1063/1.2121687

Abraham MJ, Murtola T, Schulz R, Páll S, Smith JC, Hess B, Lindahl E. (2015) **GROMACS: High performance molecular simulations through multi-level parallelism from laptops to supercomputers** *SoftwareX* **1**:19–25 https://doi.org/10.1016/j.softx.2015.06.001

Anwer MU, Boikoglou E, Herrero E, Hallstein M, Davis AM, Velikkakam James G, Nagy F, Davis SJ (2014) **Natural variation reveals that intracellular distribution of ELF3 protein is associated with function in the circadian clock** *eLife* https://doi.org/10.7554/eLife.02206

Bari KJ, Prakashchand DD (2021) **Fundamental Challenges and Outlook in Simulating Liquid–Liquid Phase Separation of Intrinsically Disordered Proteins** *The Journal of Physical Chemistry Letters* American Chemical Society :1644–1656 https://doi.org/10.1021/acs.jpclett.0c03404

Benayad Z, Bülow S, Stelzl LS, Hummer G. (2021) **Simulation of FUS Protein Condensates with an Adapted Coarse-Grained Model** *Journal of Chemical Theory and Computation* American Chemical Society :525–537 https://doi.org/10.1021/acs.jctc.0c01064

Berendsen HJC, Postma JPM, van Gunsteren WF, DiNola A, Haak JR (1984) **Molecular dynamics with coupling to an external bath** *The Journal of Chemical Physics* American Institute of Physics :3684–3690 https://doi.org/10.1063/1.448118

Best RB, Zheng W, Mittal J. (2014) **Balanced Protein-Water Interactions Improve Properties of Disordered Proteins and Non-Specific Protein Association** *Journal of chemical theory and computation* **10**:5113–5124 https://doi.org/10.1021/ct500569b

Bohn L, Huang J, Weidig S, Yang Z, Heidersberger C, Genty B, Falter-Braun P, Christmann A, Grill E. (2024) **The temperature sensor TWA1 is required for thermotolerance in Arabidopsis** *Nature* **629**:1126–1132

Box MS *et al.* (2015) **ELF3 Controls Thermoresponsive Growth in Arabidopsis** *Current Biology* **25**:194–199 https://doi.org/10.1016/j.cub.2014.10.076

von Bulow S, Tesei G, Lindorff-Larsen K. (2024) **Prediction of phase separation propensities of disordered proteins from sequence** *bioRxiv* https://doi.org/10.1101/2024.06.03.597109

Choi JM, Dar F, Pappu RV (2019) **LASSI: A lattice model for simulating phase transitions of multivalent proteins** *PLoS computational biology* https://doi.org/10.1371/journal.pcbi.1007028

Clark AK, Wilder JH, Grayson AW, Johnson QR, Lindsay RJ, Nellas RB, Fernandez EJ, Shen T. (2016) **The Promiscuity of Allosteric Regulation of Nuclear Receptors by Retinoid X Receptor** *The journal of physical chemistry B* **120**:8338–8345 https://doi.org/10.1021/acs.jpcb.6b02057

Das RK, Pappu RV (2013) **Conformations of intrinsically disordered proteins are influenced by linear sequence distributions of oppositely charged residues** *Proceedings of the National Academy of Sciences* **110** https://doi.org/10.1073/pnas.1304749110

Davey NE, Van Roey K, Weatheritt RJ, Toedt G, Uyar B, Altenberg B, Budd A, Diella F, Dinkel H, Gibson TJ (2012) **Attributes of short linear motifs** *Molecular BioSystems* The Royal Society of Chemistry :268–281 https://doi.org/10.1039/C1MB05231D

Dignon GL, Zheng W, Best RB, Kim YC, Mittal J. (2018) **Relation between single-molecule properties and phase behavior of intrinsically disordered proteins** *Proceedings of the National Academy of Sciences* Proceedings of the National Academy of Sciences :9929–9934 https://doi.org/10.1073/pnas.1804177115

Dignon GL, Zheng W, Kim YC, Mittal J. (2019) **Temperature-Controlled Liquid–Liquid Phase Separation of Disordered Proteins** *ACS Central Science* **5**:821–830 https://doi.org/10.1021/acscentsci.9b00102

González-Delgado J, Bernadó P, Neuvial P. (2024) **WARIO: Weighted families of contact maps to characterize conformational ensembles of (highly-)fiexible proteins** *Research Square* **64**

Jo S, Jiang W. (2015) **A generic implementation of replica exchange with solute tempering (REST2) algorithm in NAMD for complex biophysical simulations** *Computer Physics Communications* **197**:304–311 https://doi.org/10.1016/j.cpc.2015.08.030

Johnson QR, Lindsay RJ, Nellas RB, Fernandez EJ, Shen T. (2015) **Mapping Allostery through Computational Glycine Scanning and Correlation Analysis of Residue–Residue Contacts** *Biochemistry* American Chemical Society :1534–1541 https://doi.org/10.1021/bi501152d

Johnson QR, Lindsay RJ, Petridis L, Shen T. (2015) **Investigation of Carbohydrate Recognition via Computer Simulation** *Molecules (Basel, Switzerland)* **20**:7700–7718 https://doi.org/10.3390/molecules20057700

Johnson QR, Lindsay RJ, Shen T. (2018) **CAMERRA: An analysis tool for the computation of conformational dynamics by evaluating residue-residue associations** *Journal of computational chemistry* :1568–1578 https://doi.org/10.1002/jcc.25192

Joseph JA, Espinosa JR, Sanchez-Burgos I, Garaizar A, Frenkel D, Collepardo-Guevara R. (2021) **Thermodynamics and kinetics of phase separation of protein-RNA mixtures by a minimal model** *Biophysical Journal* **120**:1219–1230 https://doi.org/10.1016/j.bpj.2021.01.031

Joseph JA, Reinhardt A, Aguirre A, Chew PY, Russell KO, Espinosa JR, Garaizar A, Collepardo-Guevara R. (2021) **Physicsdriven coarse-grained model for biomolecular phase separation with near-quantitative accuracy** *Nature computational science* :732–743 https://doi.org/10.1038/s43588-021-00155-3

Jung JH *et al.* (2020) **A prion-like domain in ELF3 functions as a thermosensor in Arabidopsis** *Nature* **585**:256–260 https://doi.org/10.1038/s41586-020-2644-7

Kerbler SM, Wigge PA (2023) **Temperature Sensing in Plants** *Annual Review of Plant Biology* **74**:341–366 https://doi.org/10.1146/annurev-arplant-102820-102235

Khare SD, Ding F, Gwanmesia KN, Dokholyan NV (2005) **Molecular Origin of Polyglutamine Aggregation in Neurodegenerative Diseases** *PLOS Computational Biology* **1** https://doi.org/10.1371/journal.pcbi.0010030

Lajoie BR, Dekker J, Kaplan N. (2015) **The Hitchhiker's guide to Hi-C analysis: practical guidelines** *Methods (San Diego, Calif)* **72**:65–75 https://doi.org/10.1016/j.ymeth.2014.10.031

Lancaster AK, Nutter-Upham A, Lindquist S, King OD (2014) **PLAAC: a web and command-line application to identify proteins with prion-like amino acid composition** *Bioinformatics (Oxford, England)* **30**:2501–2502 https://doi.org/10.1093/bioinformatics/btu310

Lin J, Xu Y, Zhu Z. (2020) **Emerging Plant Thermosensors: From RNA to Protein** *Trends in Plant Science* **25**:1187–1189 https://doi.org/10.1016/j.tplants.2020.08.007

Lindsay RJ, Mansbach RA, Gnanakaran S, Shen T. (2021) **Effects of pH on an IDP conformational ensemble explored by molecular dynamics simulation** *Biophys Chem* **271** https://doi.org/10.1016/j.bpc.2021.106552

Lindsay RJ, Pham B, Shen T, McCord RP (2018) **Characterizing the 3D structure and dynamics of chromosomes and proteins in a common contact matrix framework** *Nucleic acids research* **46**:8143–8152 https://doi.org/10.1093/nar/gky604

Liu X, Covington M, Fankhauser C, Chory J, Wagner D. (2001) **ELF3 Encodes a Circadian Clock-Regulated Nuclear Protein That Functions in an Arabidopsis PHYB Signal Transduction Pathway** *Plant Cell* **13**:1293–1304 https://doi.org/10.1105/tpc.13.6.1293

Lotthammer JM, Ginell GM, Griffith D, Emenecker RJ, Holehouse AS (2024) **Direct prediction of intrinsically disordered protein conformational properties from sequence** *Nature Methods* https://doi.org/10.1038/s41592-023-02159-5

Mao AH, Crick SL, Vitalis A, Chicoine CL, Pappu RV (2010) **Net charge per residue modulates conformational ensembles of intrinsically disordered proteins** *Proceedings of the National Academy of Sciences* **107**:8183–8188 https://doi.org/10.1073/pnas.0911107107

Maristany MJ, Gonzalez AA, Collepardo-Guevara R, Joseph JA (2023) **Universal predictive scaling laws of phase separation of prion-like low complexity domains** *bioRxiv* https://doi.org/10.1101/2023.06.14.543914

Martin EW, Holehouse AS, Peran I, Farag M, Incicco JJ, Bremer A, Grace CR, Soranno A, Pappu RV, Mittag T. (2020) **Valence and patterning of aromatic residues determine the phase behavior of prion-like domains** *Science (New York, NY)* :694–699 https://doi.org/10.1126/science.aaw8653

Martin EW, Mittag T. (2018) **Relationship of Sequence and Phase Separation in Protein Low-Complexity Regions** *Biochemistry* American Chemical Society :2478–2487 https://doi.org/10.1021/acs.biochem.8b00008

Martin EW, Mittag T. (2018) **Relationship of sequence and phase separation in protein low-complexity regions** *Biochemistry* **57**:2478–2487

Moses D, Ginell GM, Holehouse AS, Sukenik S. (2023) **Intrinsically disordered regions are poised to act as sensors of cellular chemistry** *Trends in Biochemical Sciences* **48**:1019–1034 https://doi.org/10.1016/j.tibs.2023.08.001

Nag N, Chetri PB, Uversky VN, Giri R, Tripathi T., Tripathi T, Dubey VK (2022) **Chapter 31 - Experimental methods to study intrinsically disordered proteins** *Advances in Protein Molecular and Structural Biology Methods* Academic Press :505–533 https://doi.org/10.1016/B978-0-323-90264-9.00031-3

Nusinow DA, Helfer A, Hamilton EE, King JJ, Imaizumi T, Schultz TF, Farré EM, Kay SA (2011) **The ELF4-ELF3-LUX complex links the circadian clock to diurnal control of hypocotyl growth** *Nature* **475**:398–402 https://doi.org/10.1038/nature10182

Paik I, Huq E. (2019) **Plant photoreceptors: Multi-functional sensory proteins and their signaling networks** *Seminars in cell & developmental biology* :114–121 https://doi.org/10.1016/j.semcdb.2019.03.007

Parrinello M, Rahman A. (1980) **Crystal Structure and Pair Potentials: A Molecular-Dynamics Study** *Physical Review Letters* American Physical Society :1196–1199 https://doi.org/10.1103/PhysRevLett.45.1196

Pietrek LM, Stelzl LS, Hummer G. (2020) **Hierarchical Ensembles of Intrinsically Disordered Proteins at Atomic Resolution in Molecular Dynamics Simulations** *Journal of Chemical Theory and Computation* **16**:725–737 https://doi.org/10.1021/acs.jctc.9b00809

Quint M, Delker C, Franklin KA, Wigge PA, Halliday KJ, van Zanten M. (2016) **Molecular and genetic control of plant thermomorphogenesis** *Nat Plants* **2**

Quiroz FG, Chilkoti A. (2015) **Sequence heuristics to encode phase behaviour in intrinsically disordered protein polymers** *Nature Materials* **14**:1164–1171 https://doi.org/10.1038/nmat4418

Ramazzotti M, Monsellier E, Kamoun C, Degl'Innocenti D, Melki R. (2012) **Polyglutamine repeats are associated to specific sequence biases that are conserved among eukaryotes** *PloS one* **7** https://doi.org/10.1371/journal.pone.0030824

Regy RM, Thompson J, Kim YC, Mittal J. (2021) **Improved coarse-grained model for studying sequence dependent phase separation of disordered proteins** *Protein science : a publication of the Protein Society* :1371–1379 https://doi.org/10.1002/pro.4094

Reiner A, Dragatsis I, Dietrich P. (2011) **Genetics and neuropathology of Huntington's disease** *International review of neurobiology* :325–372 https://doi.org/10.1016/B978-0-12-381328-2.00014-6

Robustelli P, Piana S, Shaw DE (2018) **Developing a molecular dynamics force field for both folded and disordered protein states** *Proceedings of the National Academy of Sciences of the United States of America* :E4758–E4766 https://doi.org/10.1073/pnas.1800690115

Romero P, Obradovic Z, Li X, Garner EC, Brown CJ, Dunker AK (2001) **Sequence complexity of disordered protein** *Proteins: Structure, Function, and Bioinformatics* **42**:38–48 https://doi.org/10.1002/1097-0134(20010101)42:1<38::AID-PROT50>3.0.CO;2-3

Ruff KM, Roberts S, Chilkoti A, Pappu RV (2018) **Advances in Understanding Stimulus-Responsive Phase Behavior of Intrinsically Disordered Protein Polymers** *Journal of Molecular Biology* **430**:4619–4635 https://doi.org/10.1016/j.jmb.2018.06.031

Schramm A, Bignon C, Brocca S, Grandori R, Santambrogio C, Longhi S. (2019) **An arsenal of methods for the experimental characterization of intrinsically disordered proteins – How to choose and combine them?** *Archives of Biochemistry and Biophysics* **676** https://doi.org/10.1016/j.abb.2019.07.020

Sengupta P, Garrity P. (2013) **Sensing temperature** *Current Biology* **23**:R304–R307 https://doi.org/10.1016/j.cub.2013.03.009

Song D, Luo R, Chen HF (2017) **The IDP-Specific Force Field ff14IDPSFF Improves the Conformer Sampling of Intrinsically Disordered Proteins** *Journal of Chemical Information and Modeling* American Chemical Society :1166–1178 https://doi.org/10.1021/acs.jcim.7b00135

Stelzl LS, Pietrek LM, Holla A, Oroz J, Sikora M, Köfinger J, Schuler B, Zweckstetter M, Hummer G. (2022) **Global Structure of the Intrinsically Disordered Protein Tau Emerges from Its Local Structure** *JACS Au* American Chemical Society :673–686 https://doi.org/10.1021/jacsau.1c00536

Tesei G, Lindorff-Larsen K. (2022) **Improved predictions of phase behaviour of intrinsically disordered proteins by tuning the interaction range** *Open research Europe* https://doi.org/10.12688/openreseurope.14967.2

Tesei G, Schulze TK, Crehuet R, Lindorff-Larsen K. (2021) **Accurate model of liquid-liquid phase behavior of intrinsically disordered proteins from optimization of single-chain properties** *Proceedings of the National Academy of Sciences of the United States of America* https://doi.org/10.1073/pnas.2111696118

Thines B, Harmon FG (2010) **Ambient temperature response establishes ELF3 as a required component of the core Arabidopsis circadian clock** *Proceedings of the National Academy of Sciences* Proceedings of the National Academy of Sciences :3257–3262 https://doi.org/10.1073/pnas.0911006107

Thomasen FE, Pesce F, Roesgaard MA, Tesei G, Lindorff-Larsen K. (2022) **Improving Martini 3 for Disordered and Multidomain Proteins** *Journal of Chemical Theory and Computation* American Chemical Society :2033–2041 https://doi.org/10.1021/acs.jctc.1c01042

Totzeck F, Andrade-Navarro MA, Mier P. (2017) **The Protein Structure Context of PolyQ Regions** *PloS one* **12** https://doi.org/10.1371/journal.pone.0170801

Valley CC, Cembran A, Perlmutter JD, Lewis AK, Labello NP, Gao J, Sachs JN (2012) **The methionine-aromatic motif plays a unique role in stabilizing protein structure** *The Journal of biological chemistry* :34979–34991 https://doi.org/10.1074/jbc.M112.374504

Vernon RM, Chong PA, Tsang B, Kim TH, Bah A, Farber P, Lin H, Forman-Kay JD (2018) **Pi-Pi contacts are an overlooked protein feature relevant to phase separation** *eLife* **7** https://doi.org/10.7554/eLife.31486

Viegas RG, Martins IBS, Sanches MN, Oliveira Junior AB, JBd Camargo, Paulovich FV, Leite VBP (2024) **ELViM: Exploring biomolecular energy landscapes through multidimensional visualization** *J Chem Inf Model* **64**:3443–3450

Wang L, Friesner RA, Berne BJ (2011) **Replica exchange with solute scaling: a more efficient version of replica exchange with solute tempering (REST2)** *J Phys Chem B* **115**:9431–9438

Wang L, Friesner RA, Berne BJ (2011) **Replica exchange with solute scaling: a more efficient version of replica exchange with solute tempering (REST2)** *The journal of physical chemistry B* **115**:9431–9438 https://doi.org/10.1021/jp204407d

Wu H, Wolynes PG, Papoian GA (2018) **AWSEM-IDP: A Coarse-Grained Force Field for Intrinsically Disordered Proteins** *The Journal of Physical Chemistry B* **122**:11115–11125 https://doi.org/10.1021/acs.jpcb.8b05791

Zagotta M, Shannon S, Jacobs C, Meeks-Wagner D. (1992) **Early-Flowering Mutants of Arabidopsis thaliana** *Functional Plant Biology* **19**:411–418 https://doi.org/10.1071/PP9920411

Zhang C *et al.* (2019) **LUX ARRHYTHMO mediates crosstalk between the circadian clock and defense in Arabidopsis** *Nature Communications* **10** https://doi.org/10.1038/s41467-019-10485-6

Zhang Y, Chen J. (2022) **Recalibrating replica exchange solute tempering for sampling disordered protein conformations** *Biophysical Journal* Elsevier https://doi.org/10.1016/j.bpj.2021.11.1730

Zhao C *et al.* (2017) **Temperature increase reduces global yields of major crops in four independent estimates** *Proceedings of the National Academy of Sciences* **114**:9326–9331 https://doi.org/10.1073/pnas.1701762114

Author information

Richard J Lindsay
Center for Computational Biology, Flatiron Institute, New York, USA, Center for Computational Mathematics, Flatiron Institute, New York, USA

Rafael Giordano Viegas
Department of Physics, São Paulo State University (UNESP), Institute of Biosciences, Humanities and Exact Sciences, São Paulo, Brazil, Federal Institute of Education, Science and Technology of São Paulo (IFSP), São Paulo, Brazil

Vitor BP Leite
Department of Physics, São Paulo State University (UNESP), Institute of Biosciences, Humanities and Exact Sciences, São Paulo, Brazil
ORCID iD: 0000-0003-0008-9079

Philip A Wigge
Leibniz-Institut für Gemüse-und Zierpflanzenbau, Großbeeren, Germany, Institute of Biochemistry and Biology, University of Potsdam, Potsdam, Germany
ORCID iD: 0000-0003-4822-361X

Sonya M Hanson
Center for Computational Biology, Flatiron Institute, New York, USA, Center for Computational Mathematics, Flatiron Institute, New York, USA

For correspondence: shanson@flatironinstitute.org

Editors

Reviewing Editor
Qiang Cui
Boston University, Boston, United States of America

Senior Editor
Qiang Cui
Boston University, Boston, United States of America

Reviewer #1 (Public review):

Summary:

This manuscript explores the role of the Evening Complex (EC), specifically focusing on ELF3, a disordered protein component of the EC, and its temperature-dependent phase behavior. The study highlights the role of polyQ tracts in modulating temperature-sensitive condensate formation and provides a combination of computational approaches, including REST2 simulations and coarse-grained Martini simulations, to investigate how polyQ tract length and sequence context influence this behavior.

Strengths:

The study addresses a key question in plant biology - how temperature influences circadian clock-mediated growth regulation through protein phase behavior. The manuscript introduces the novel finding that polyQ tract length modulates the temperature-dependent formation of helices and condensates.

Weaknesses:

(1) Coarse-Grained Simulation Results Not Supported by Data:
The results presented in Figure 6A of the manuscript do not seem to show a clear trend in the number of clusters formed as a function of polyQ tract length. This is particularly evident in the comparison between 0Q and 7Q polyQ lengths, which display statistically similar values in terms of the number of clusters. The lack of distinction between these values raises questions about the sensitivity of the coarse-grained simulations to polyQ tract length, which the authors claim as a key modulator of condensate formation. This discrepancy weakens the argument that polyQ length directly impacts the clustering behavior in the simulations.
Suggested Analysis:
- A more detailed statistical analysis should be performed to assess whether the observed differences between polyQ lengths are significant. This could involve hypothesis testing or the use of error bars in the graphs to better communicate the variability in the data.
- Additionally, the authors should examine whether there are other features, such as cluster shape or internal structure, that might differentiate between different polyQ lengths, even if the total number of clusters is similar.

(2) Inconsistency in Cluster Size Across Temperatures (Figure 6B):
The results in Figure 6B show a striking difference in the size of the largest cluster between temperatures of 290K and 300K. This abrupt shift in behavior lacks a clear mechanistic explanation. Typically, phase transitions driven by temperature are more gradual, unless there is some underlying structural or chemical shift that the authors have not accounted for. Without a clear explanation, this sudden change in behavior reduces confidence in the simulation results.
Suggested Analysis:
- The authors should explore possible explanations for the dramatic difference in cluster size between 290K and 300K. For example, they could investigate whether specific interactions (such as the breaking or formation of hydrogen bonds or hydrophobic contacts) might explain the behavior at higher temperatures.
- It is important to check whether the coarse-grained simulation model has been adequately parameterized and scaled for accurate temperature dependence. Atomistic simulations of monomers and dimers with varying polyQ tract lengths could be used to fine-tune the coarse-grained model, ensuring it accurately reflects molecular behavior. The gross estimate of a

10% scaling factor might be insufficient and could lead to inaccurate representations of cluster formation.

(3) Scaling of Coarse-Grained Model with Atomistic Simulations:
As mentioned, the coarse-grained model used in the study may not have been properly scaled against atomistic data. A simple scaling factor of 10% may not be appropriate for accurately capturing the behavior of polyQ tracts across different lengths, especially considering their sensitivity to subtle changes in temperature. Without rigorous validation against atomistic simulations, the coarse-grained model's predictions could be skewed.
Suggested Analysis:

(4) To address this, the authors should compare the coarse-grained model with atomistic simulations of monomeric and dimeric forms of ELF3 with different polyQ tract lengths. By comparing key structural parameters (e.g., radius of gyration, contact maps, and clustering propensity), the authors could adjust the coarse-grained model to more accurately reflect the atomistic behavior. The authors have wealth of atomistic simulation data that could afford such benchmarking and identification of scaling factor
o Additionally, the authors should investigate whether the assumed scaling factor of 10% is appropriate for each polyQ length or whether it needs to be refined based on specific properties, such as the number of hydrophobic interactions or secondary structure stability.

(5) Lack of Analysis for Liquid-Like Behavior in Phase Separation:
The simulations presented in the manuscript do not analyze the liquid-like behavior of ELF3 condensates, which is a key characteristic of liquid-liquid phase separation (LLPS). In LLPS systems, condensates are often dynamic, with chains exchanging between clusters, indicating liquid-like rather than solid-like behavior. The authors fail to probe this crucial aspect, which is necessary to support the claim that ELF3 undergoes phase separation.
Suggested Analysis:
- The authors should conduct additional analyses to probe the liquid-like nature of the clusters formed by ELF3. One approach would be to analyze the dynamics of chain exchange between clusters, measuring how frequently chains leave one cluster and join another over time. This analysis would reveal whether the condensates behave as liquid-like, dynamic structures or more static, solid-like aggregates.
- Additionally, the temperature dependence of these exchange dynamics should be investigated. In true liquid-liquid phase separation, the rate of chain exchange is often sensitive to temperature. Observing how this rate changes between 290K and 300K, for instance, could help explain the abrupt shift in cluster size seen in Figure 6B.
- The authors should also analyze whether the internal structures of the condensates are consistent with a liquid-like phase. For example, radial distribution functions and contact lifetimes could be calculated to reveal whether the clusters exhibit liquid-like organization.

(6) Lack of justification of polydispersity of polyQ:
The authors don't provide any rationale for choice of different copies of polyQ used in the manuscript for their chain-growth simulation studies. It will be more apt if it can be motivated via some precedent experimental observations.

(7) Lack of initiative to connect to Experiments:
While the computational models and simulations provide robust theoretical insights, the absence of direct experimental validation weakens the overall impact of the manuscript. For example, experimental data on how specific mutations in the polyQ tract influence ELF3 behavior in vivo would significantly bolster the authors' claims. The manuscript would benefit from either citing existing experimental studies that corroborate these findings or from suggesting future experimental directions.

https://doi.org/10.7554/eLife.102410.1.sa2

Reviewer #2 (Public review):

Summary:

The authors aimed to explore how a key protein in the circadian clock of plants, ELF3, responds to temperature changes by forming molecular condensates. They focused on understanding the role of a specific region of the protein, a polyQ tract, in promoting temperature-sensitive structural changes and regulating the formation of condensates. Through a series of computational simulations, they sought to uncover the molecular basis for ELF3's temperature responsiveness and its broader implications for plant growth and adaptation to environmental conditions.

Strengths:

The study's strength lies in its focus on an important biological question: how plants sense and respond to temperature changes at the molecular level. The authors employed a variety of computational techniques, including coarse-grained simulations, to explore the role of specific molecular features in this process. These methods provide a multi-scale view of protein behavior and offer valuable insights into how molecular structures may influence biological function.

Weaknesses:

However, there are notable weaknesses in the evidence provided. While the authors present trends in molecular changes, such as shifts in helical propensity and the formation of condensates, these results seem subtle and are not strongly substantiated by statistical analysis. The lack of error bars in the figures makes it difficult to distinguish between meaningful signals and potential noise in the data. Furthermore, the temperature-sensitive behavior appears to be influenced more by chain length than by sequence-specific effects of the polyQ region, raising questions about whether the findings truly capture the molecular mechanisms responsible for temperature sensing. Additionally, some simulations, particularly those related to the formation of condensates, do not appear fully converged, which casts further doubt on the robustness of the results.

Additional Context for Readers:

Readers should interpret the results with caution, especially regarding the molecular mechanisms proposed for temperature sensing. While the study presents interesting trends, the evidence is not definitive, and the findings may be more reflective of general protein behavior (such as the effect of chain length on condensate formation) than specific sequence-driven responses to temperature. Further experimental studies and more converged simulations will be necessary to fully understand the role of ELF3 in temperature regulation.

https://doi.org/10.7554/eLife.102410.1.sa1

Author response:

We sincerely thank the reviewers for their constructive feedback and the editor for facilitating this thorough review. We found the suggestions insightful and valuable for refining our manuscript. We would like to clarify a few points in an initial response before presenting the fully updated manuscript. First of all, we would like to emphasize the multi-scale nature of our approach, where we derived insights from both atomistic and coarse-grained simulations. Reviewers focused mostly on the coarse-grained simulations, the drawbacks of which we are aware and were a strong motivation for starting with the atomistic approach. Reviewer 1 mentioned a lack of a proposed mechanism for the increased

condensate forming propensity at 300K vs. 290K, and we feel we had clearly pointed to the aromatic contacts as a mechanism for this, but we will make sure to clarify this further in the revision. Furthermore, reviewer 1 was critical of our use of the 10% adjustment to Martini protein-water interactions, which has previously been thoroughly presented and assessed in the literature (see for example Tesei et al *JCTC* 2022). Furthermore, for our specific system we were encouraged by the favorable comparison of our Martini simulations to the atomistic simulations, e.g. for radius of gyration, contact propensity, and solvent accessibility. We will make sure to emphasize this more clearly in the revision. Finally, we are grateful for the feedback from both reviewers and will use their comments as a guide to incorporate additional analyses and extended simulations to strengthen our conclusions in an upcoming revision.

https://doi.org/10.7554/eLife.102410.1.sa0